12 (2022) 100221

Contents lists available at ScienceDirect

Biosensors and Bioelectronics: X

journal homepage: www.journals.elsevier.com/biosensors-and-bioelectronics-x

Infrared photoelectrochemical sensing of urea with silicon photoanodes

Joudi Dabboussi [a,1], Yiran Zhao [a,1], Rawa Abdallah [b], Albane Gicquel [c], Claude Bendavid [c,d], Gabriel Loget [a,*]

[a] Univ Rennes, CNRS, ISCR (Institut des Sciences Chimiques de Rennes)-UMR6226 Rennes F-35000, France
[b] Lebanese University, EDST, AZM Center for Research in Biotechnology and Its Applications Laboratory of Applied Biotechnology, LBA3B, El Mitein Street, Tripoli, Lebanon
[c] INSERM, INRAE, Université de Rennes, Nutrition Metabolisms and Cancer, Rennes, St Gilles, France
[d] Laboratoire de Biochimie Toxicologie, Pôle Biologie, CHU de Rennes, Rennes, France

ARTICLE INFO

Keywords:
Photoelectrochemical sensing
Silicon
Photoanode
Urea oxidation reaction
Nickel
Urine

ABSTRACT

Urea is an essential molecule for life and the environment. In particular, in biological fluids, the urea concentration can be indicative of several pathologies. Herein, we propose a photoelectrochemical system activated by infrared irradiation (850 nm) for the detection of urea. Our sensor is made of a photoactive Si photoanode protected by a silicon oxide/Ni thin film and is coated with a Ni–Mo–O film that catalyzes the urea oxidation reaction. This approach is employed for the sensitive quantification of urea, and the operation of the system in a wide range of concentrations (from μM to 10 mM) is demonstrated, revealing a sub-μM limit of detection. Sensing is performed at a constant potential of 0.24 V vs Hg/HgO under infrared illumination, and the photocurrent output depends on the urea concentration. This new device has good reliability for urea analysis in alkaline aqueous solutions. The method is tested in the determination of the urea concentration in human urine samples, and the results are compared with a reference enzymatic photochemistry assay. The method is promising for the analysis of urine samples and can open new doors in biosensing and environmental analysis.

1. Introduction

As one of the major metabolic products of protein metabolism processes in living organisms, urea is considered a primary source of organic nitrogen in soils (David L. Nelson and Cox, 2021). It is used as a fertilizer in agricultural production (Gooding and Davies, 1992) and also as a raw material for the manufacturing of a myriad of products on an industrial scale (Urbańczyk et al., 2016). Clearly, monitoring the concentration of urea is highly important for processes in agricultural chemistry, food and pharmaceutical industries, and environmental protection (Botewad et al., 2021; Pundir et al., 2019). On the other hand, for mammals, the hepatic urea cycle is the main pathway to detoxify ammonium, a toxic molecule resulting from amino acid catabolism, generating urea that is eliminated from the body almost exclusively by the kidneys via urine, allowing 80–90% of nitrogen expulsion. In this context, urea quantification is an important indicator in biomedical and clinic analysis to test renal and hepatic function. A high urea concentration in urine may indicate excessive protein consumption or excessive protein processing in the body. Conversely, a low urinary concentration may suggest severe malnutrition or a kidney malfunction (associated with high blood concentration). Subsequently, an increase in the urea level in the body can damage cells. A broad set of analytical methods, based on chromatography, fluorimetry, colorimetry, and chemiluminescence have been used for urea sensing (Botewad et al., 2021; Pundir et al., 2019). However, these methods are considered expensive and time-consuming. Recently, electrochemical urea sensors have been widely developed because of their remarkable advantages and practical application such as small size, high sensitivity, high selectivity, low detection limit, low fabrication cost, and portability (Liu et al., 2021; Nguyen et al., 2016; Tyagi et al., 2013; Yoon et al., 2017). Most urea sensing methods are based on enzymes, known to have a highly specific binding and good catalytic activity (especially urease), that hydrolyzes urea. However, enzymes are sensitive to temperature, humidity, and chemical environment and their denaturation may result in sensor instability. Non-enzymatic sensors that use inorganic catalysts for reacting with urea could overcome such drawbacks. Among them,

* Corresponding author.
E-mail address: gabriel.loget@cnrs.fr (G. Loget).
[1] These authors contributed equally.

https://doi.org/10.1016/j.biosx.2022.100221
Received 21 June 2022; Received in revised form 4 August 2022; Accepted 11 August 2022
Available online 28 August 2022

Ni-based electrodes have demonstrated excellent performance for the electrocatalytic oxidation of molecules such as urea (Boggs et al., 2009) and glucose (Mu et al., 2011; Yang et al., 2017).

On the other hand, the current developments in photo-electrochemical (PEC) sensing promise high-level analytic devices thanks to the combination of photochemistry and electrochemistry (Shu and Tang, 2020; Wang et al., 2020; Zhao et al., 2018). PEC sensing allows decoupling of the detection signal (current) with the excitation (incident light), which can be beneficial for increasing the signal-to-noise ratio thus the limit of detection with respect to electrochemical sensors. The PEC detection signal originates from the photons-to-electrons conversion at a photoactive interface involving generally a semiconductor photoelectrode. In a conventional PEC analysis system, the external light is the excitation source, and the photocurrent density is the output signal. Recently, TiO_2-based surfaces were employed for the PEC sensing of urea (Yang et al., 2020) and for dialysate regeneration (Shao et al., 2019). The appearance of new materials and junctions, which possess special advantages in optical properties and electrical conductivity, has opened new doors for the development of PEC sensors (Li et al., 2021a; Saada et al., 2020; Shu et al., 2018; Zhou et al., 2021). Specifically, electrodes based on Si can be considered one of the best candidates for PEC application because, in addition to Si's ubiquity in current technological applications, it has a suitable band structure, a narrow bandgap (1.1 eV) allowing high carrier mobility, and a good absorption from the UV to the IR region. In contrast with most PEC sensing devices based on UV or visible light, using IR light can be seen as beneficial as it grants high capacity for deep tissue penetration, minimal damage to biological species, and low spectral interference (Li et al., 2022). However, a strong challenge in the use of Si photoelectrodes resides in its low stability caused by corrosion, which is particularly pronounced when used as a photoanode (Bae et al., 2017; Sun et al., 2014). In the frame of solar energy research, progress has been made in solving this challenge (Loget, 2019). Recently, our group reported the preparation and the characterization of *n*-type Si (*n*-Si)-based junctions comprising a protective and a catalytic coating that are active toward urea for hours under simulated sunlight (Dabboussi et al., 2022). In this paper, we investigate these photoanodes for a new application, namely urea detection. We use IR illumination as an excitation source, which differs from the previous use of these photoanodes, and we perform proof-of-concept experiments to evaluate their potential utilization in biomedical applications. This work constitutes the first step towards the elaboration of Si-based photoelectrochemical sensors for urea detection in several media.

2. Results and discussion

Oxide catalysts containing Ni and Mo are known to be highly active for urea oxidation (Sha et al., 2020; Yu et al., 2018; Zhang et al., 2019), a mechanism that is promising in the context of solar energy conversion (Loget et al., 2019; Wang et al., 2012), and also for urea sensing, as discussed in the following. Although it has been recently reported that several reaction pathways exist for urea oxidation (Li et al., 2021b), here, we only consider the urea oxidation reaction (UOR) written below as **Reaction 1**.

$$(NH_2)_2CO\ (aq) + 6\ OH^-\ (aq) + 6\ h^+ \rightarrow N_2\ (g) + 5\ H_2O\ (l) + CO_2\ (g) \quad (1)$$

Lately, our group reported the preparation and the characterization of photoanodes based on the *n*-Si/SiO_x/Ni metal-insulator-semiconductor (MIS) architecture (Kenney et al., 2013; Loget et al., 2019; Zhao et al., 2019), onto which an amorphous catalytic Ni–Mo–O (NMO) coating is deposited (Dabboussi et al., 2022). The preparation method, described in detail in **Section S1** consists, in short, in first depositing a Ni metal thin film onto Si/SiO_x and then modifying *n*-Si/SiO_x/Ni with the NMO coating by a hydrothermal method followed by an Ar annealing step. In this construct, depicted in Fig. 1a, SiO_x/Ni grants protection to Si towards photocorrosion, Ni is the charge collector and NMO is the catalytic coating for UOR (Dabboussi et al., 2022).

Scanning electron microscopy (SEM) images, shown in Fig. 1b and c revealed that, after deposition, the NMO coating is an 80 nm-thick porous layer covering the *n*-Si/SiO_x/Ni surface. The Ni-to-Mo atomic ratio, determined by EDS (Fig. S1) is 9, in good agreement with our previous report (Dabboussi et al., 2022). As previously discussed by our group in the context of UOR and by others in the context of alkaline oxygen evolution reaction (OER) (Dürr et al., 2021; Liu et al., 2020), Mo is a structuring agent which promotes the growth of the NMO coating (Dabboussi et al., 2022) and the formation of a high density of Ni$(OH)_2$/NiOOH reactive sites for UOR by dissolving into the electrolyte. This was confirmed by our EDS analysis as described in **Section S2**. For simplicity's sake, the *n*-Si/SiO_x/Ni/NMO photoanode is referred to as the Si photoanode in the rest of the article. The PEC experiments were performed in a three-neck PEC cell, allowing for illuminating the Si photoanode with an 850 nm IR light-emitting diode (LED), as described in **Section S1**. The power of the LED is 10 mW cm^{-2} and the spectrum is presented in Fig. S2. The electrolyte is a 10 mL solution of 1 M KOH and the Si photoanode is illuminated from the catalyst side, as shown in Fig. 1a. The cyclic voltammograms (CVs) shown in Fig. 1e demonstrate the effects of the presence of urea and the illumination. Only negligible current is measured in the dark (blue CV), while illumination promotes the generation of higher currents. In the absence of urea (red CV), the oxidation wave corresponds to the conversion of $Ni(OH)_2$ in NiOOH (peak at 0.13 V, all potentials in this article are referred vs Hg/HgO (1 M KOH)) (Hall et al., 2013; Medway et al., 2006) and the following increase in photocurrent density is attributed to OER. In the presence of urea, the photocurrent density at low overpotentials is much higher due to the UOR (**Reaction (1)**), which occurs as soon as $Ni(OH)_2$ is converted into NiOOH, by an electrochemical-chemical (EC) mechanism (Vedharathinam and Botte, 2013). These results are in good agreement with that reported with a polychromatic illumination (Dabboussi et al., 2022). The difference in CV characteristics, observed with and without urea in Fig. 1e suggests that this photoanode can be employed for urea sensing, which will be evaluated next.

PEC sensing was performed at a constant bias of 0.24 V (grey dotted line in Fig. 1e). Fig. 2a presents a representative chronoamperogram (CA) recorded during PEC sensing of urea. After equilibration of the photocurrent density (j) to a j_0 value (inset of Fig. 2a) corresponding to residual OER (0.28 mA cm^{-2}), 100 μL of the urea stock solution was sequentially injected into the cell and current was simultaneously recorded. After injection, the electrolyte was rapidly homogenized by stirring, which induced the large spikes due to an increased urea mass transport to the electrode. The stabilized j corresponds to the steady-state value for OER and UOR. As shown in Fig. 2a, j increased with urea concentration. Concentrations above 10 mM were not studied as they often led to a strong deviation from linearity, as shown in Fig. 2a.

Calibration curves, presented in Fig. 2b–e, were determined as the UOR photocurrent density (j-j_0) in four concentration ranges (1–10 μM, 10–100 μM, 0.1–1 mM, and 1–10 mM). These curves show a linear response in all cases, with sensitivity values of 5009, 424.3, 90.5, and 70.4 mA cm^{-2} M^{-1} and coefficients of determination $R^2 \geq 0.97$. As shown in the inset of Fig. 2a, the method allowed us to easily measure a concentration of 1 μM, and, according to the electrochemical noise level during the measurement, we can estimate that a limit of detection (LOD, S/N = 3) of 350 nM is reachable (Fig. S3). To the best of our knowledge, this constitutes the first report on urea PEC sensing and, as shown in Table S1, the LOD reported here is lower than several LOD previously reported electrochemical sensors (Ahmad et al., 2014; Amin et al., 2019; Ansari et al., 2015; Nguyen et al., 2016; Pan and Lin, 2009). As shown in Fig. S4, The stability of the photoanode was assessed for ~2 h under intermittent illumination and a constant concentration. Repeatability experiments were performed with seven independently prepared Si photoanodes, the relative standard deviations (RSD) measured in the four concentration ranges are presented in Table S2.

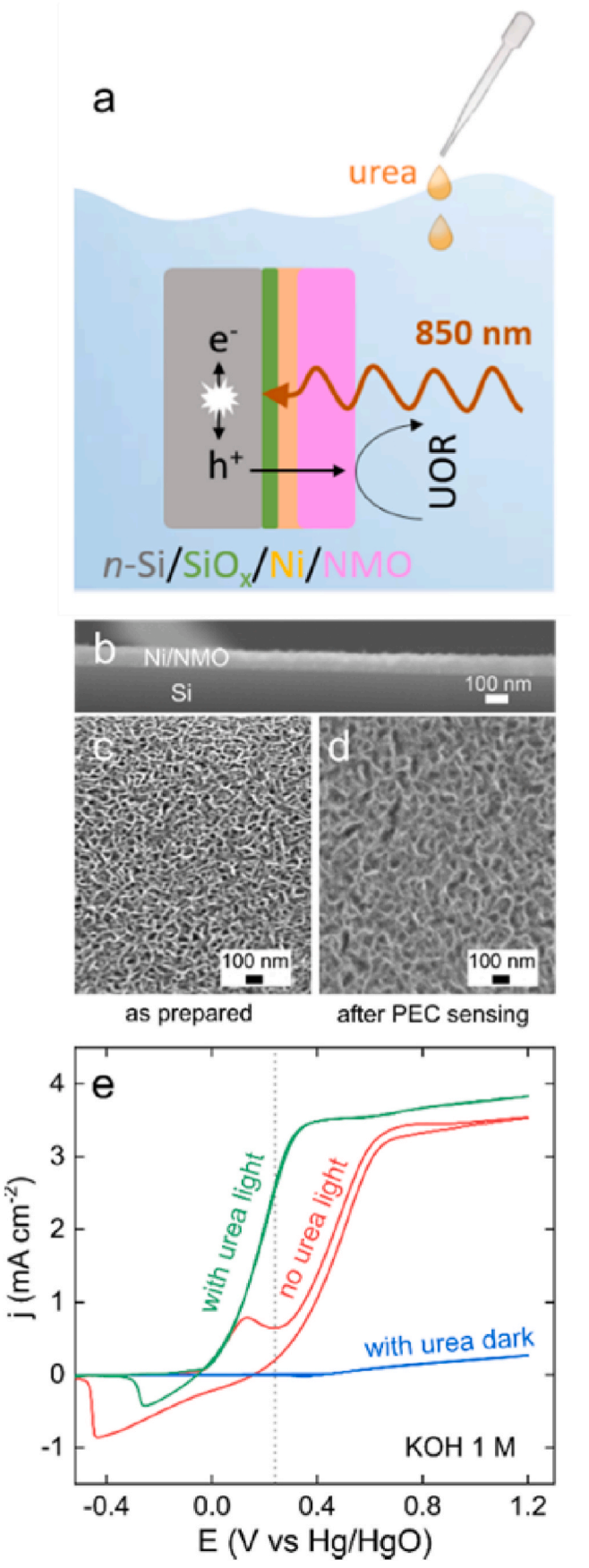

(caption on next column)

Fig. 1. a) Scheme showing a Si photoanode under IR illumination during urea sensing. **b)** SEM cross-section view of a Si photoanode. **c,d)** SEM top views of Si photoanodes, after preparation (c) and after urea sensing with urine samples (d). **e)** CVs recorded with the Si photoanode in 1 M KOH under 850 nm illumination without urea (red curve), with 0.1 M urea in the dark (blue curve), and with 0.1 M urea under 850 nm illumination (green curve), the scan rate is 20 mV s^{-1}. The grey dotted line indicates the potential (0.24 V) that is used for urea sensing. (For interpretation of the references to color in this figure legend, the reader is referred to the Web version of this article.)

To evaluate the possibility of using our Si photoanodes for relevant samples, we tested our method for urea sensing with ten human urine samples obtained from a hospital medical laboratory. To do so, the calibration curve of a photoanode was first determined, then, the urine samples were centrifuged to remove any aggregates before analysis and then diluted by a 1 M KOH solution to reach a urea concentration in the 0.1–1 mM range. Fig. 3a shows the urea concentration obtained for each sample by the PEC method (white bars) and that obtained by a reference enzymatic colorimetric assay method (grey bars, details are provided in **Section S1**). In Fig. 3b, the urea concentration measured by PEC sensing is plotted as a function of that measured by the reference method, the grey dashed curve represents the identity function ($y = x$) and the deviation from that curve indicates the reliability for a given sample. Even if the population ($n = 10$) is too low to precisely determine the reliability of our method, we can see that the PEC method was valid for 7 samples and that 3 samples gave erroneous data (#1, #3, and #7). We postulate that higher PEC values are obtained when a compound (or several) in the sample is oxidized concomitantly with urea to produce a higher overall j output (e.g., #1, #7). Conversely, in #3, the PEC value is lower than the reference value, which can be attributed to the adsorption of entities present in the biological sample onto the photoanode surface. Finally, the surface of the Si photoanode used for the PEC sensing of urea in urine was characterized by SEM and EDS, the results, presented in Fig. 1d and Fig. S1, show that the catalytic coating was still present on the surface after the sensing experiments.

3. Conclusion

In conclusion, silicon photoanodes comprising a protective SiO_x/Ni layer and a Ni–Mo–O catalytic coating have been developed for urea PEC sensing under potentiostatic control with IR irradiation (850 nm). Our study showed that this system grants four linear photocurrent responses corresponding to four orders of magnitudes of urea concentration (1 μM–10 mM). The sensor can operate with good stability (Fig. S4), which presents a challenge for Si-based photoanodes. Preliminary results suggest that such photoanodes may be employed for the sensing of urea in human urine and that progress can be further made by suppressing undesired processes such as fouling or oxidation of interferents. The next step would be to perform a systematic study with a larger number of urine samples and to elucidate the interfering reactions and phenomena detrimental to measurements in biological samples. In addition, this system should be tested for urea sensing in more complex biological matrices such as blood, sweat, and duodenal fluids. Benefitting from its activity in the IR region, it could also be promising for urea sensing through tissues.

CRediT authorship contribution statement

Joudi Dabboussi: Methodology, Formal analysis, Writing – original draft, Writing – review & editing. **Yiran Zhao:** Methodology, Formal analysis, Writing – original draft, Writing – review & editing. **Rawa Abdallah:** Project administration, Writing – original draft. **Albane Gicquel:** Resources, Visualization. **Claude Bendavid:** Formal analysis, Conceptualization, Resources. **Gabriel Loget:** Conceptualization, Methodology, Writing – original draft, Writing – review & editing, Visualization, Supervision, Project administration, Funding acquisition.

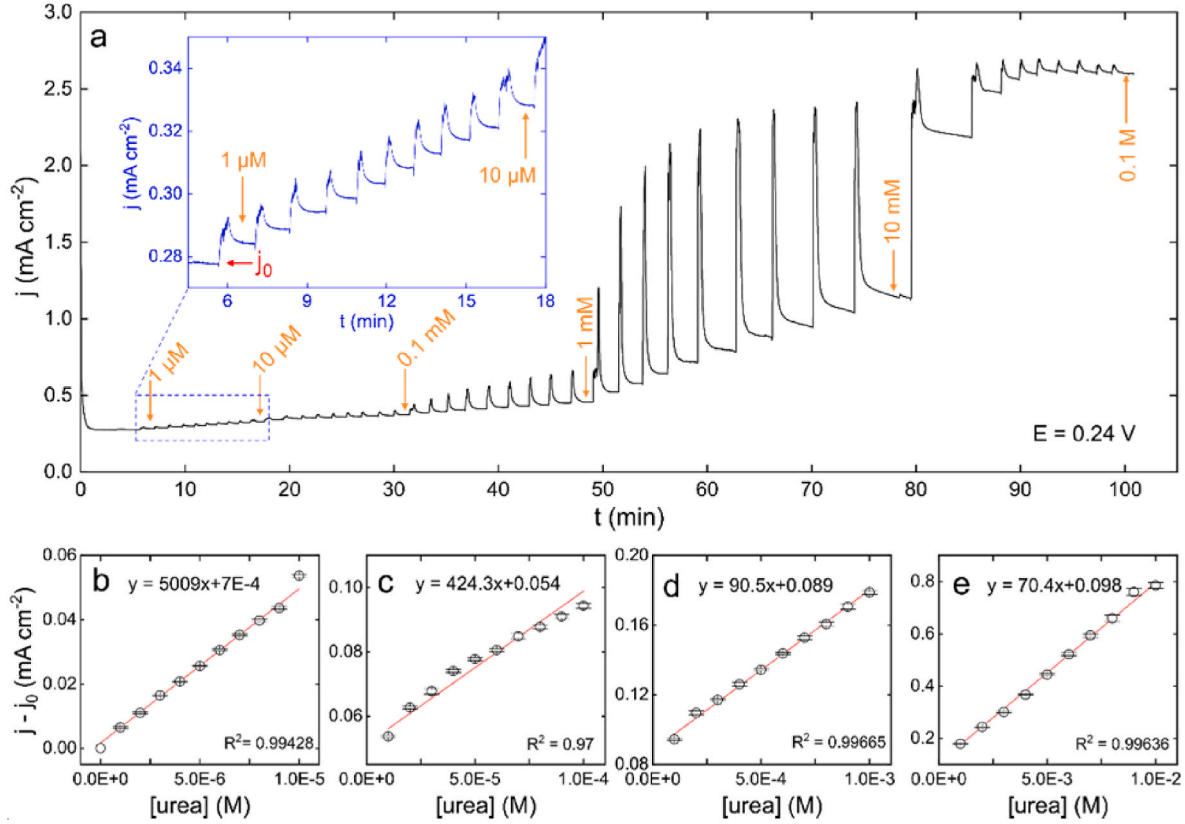

Fig. 2. a) Chronoamperogram recorded on a Si photoanode under 850 nm illumination in 1 M KOH with an increasing concentration of urea (from 1 µM to 0.1 M) at an applied bias of 0.24 V. Inset: detail of 1-to-10 µM range. **b-e)** Calibration curves, presented as j-j_0 as a function of the urea concentration in different ranges. From 1 to 10 µM (b), from 10 to 100 µM (c), from 0.1 to 1 mM (d) and from 1 to 10 mM (e). The error bars equal two standard deviations (see Section S1 for more details), red curves are linear fits. (For interpretation of the references to color in this figure legend, the reader is referred to the Web version of this article.)

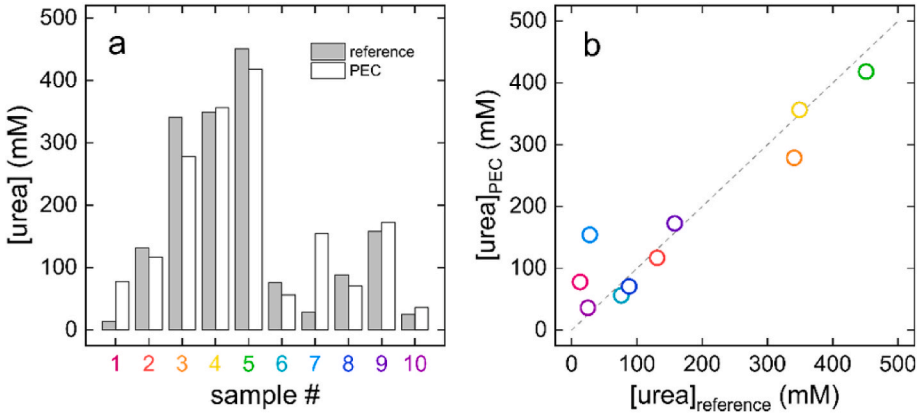

Fig. 3. a) Urea concentration determined for ten human urine samples by the reference method (grey bars) and by PEC sensing with the Si photoanode (white bars). **b)** Plot of the urea concentration values determined by photoelectrochemical sensing with the Si photoanode as a function of that determined by the reference method. The grey dashed line represents the identity function. The colors of the disks in 3b correlate with sample # in 3a. (For interpretation of the references to color in this figure legend, the reader is referred to the Web version of this article.)

Declaration of competing interest

The authors declare that they have no known competing financial interests or personal relationships that could have appeared to influence the work reported in this paper.

Acknowledgments

This work is supported by the Fondation Grand Ouest. Francis Gouttefangeas from ScanMAT/CMEBA is acknowledged for SEM analyses.

Appendix A. Supplementary data

Supplementary data to this article can be found online at https://doi.org/10.1016/j.biosx.2022.100221.

References

Ahmad, R., Tripathy, N., Hahn, Y.-B., 2014. Sensor. Actuator. B Chem. 194, 290–295.
Amin, S., Tahira, A., Solangi, A., Beni, V., Morante, J.R., Liu, X., Falhman, M., Mazzaro, R., Ibupoto, Z.H., Vomiero, A., 2019. RSC Adv. 9, 14443–14451.
Ansari, S.G., Fouad, H., Shin, H.-S., Ansari, Z.A., 2015. Chem. Biol. Interact. 242, 45–49.
Bae, D., Seger, B., Vesborg, P.C.K., Hansen, O., Chorkendorff, I., 2017. Chem. Soc. Rev. 46, 1933–1954.
Boggs, B.K., King, R.L., Botte, G.G., 2009. Chem. Commun. 4859–4861.

Botewad, S.N., Gaikwad, D.K., Girhe, N.B., Thorat, H.N., Pawar, P.P., 2021. Biotechnol. Appl. Biochem. 1–17.
Dabboussi, J., Abdallah, R., Santinacci, L., Zanna, S., Vacher, A., Dorcet, V., Fryars, S., Floner, D., Loget, G., 2022. J. Mater. Chem. https://doi.org/10.1039/D2TA01212J (in press).
Dürr, R.N., Maltoni, P., Tian, H., Jousselme, B., Hammarström, L., Edvinsson, T., 2021. ACS Nano 15, 13504–13515.
Gooding, M.J., Davies, W.P., 1992. Fert. Res. 32, 209–222.
Hall, D.S., Bock, C., MacDougall, B.R., 2013. J. Electrochem. Soc. 160, F235–F243.
Kenney, M.J., Gong, M., Li, Y., Wu, J.Z., Feng, J., Lanza, M., Dai, H., 2013. Science 342, 836–841.
Li, H., Han, M., Weng, X., Zhang, Y., Li, J., 2021a. ACS Nano 15, 1710–1717.
Li, J., Li, J., Chen, L., Li, Y., Wang, H., Chen, X., Gong, M., Liu, Z.P., Yang, X., Hao, Y., Zhang, Y., Chen, S., Xu, M., Zhou, Y., 2021b. Angew. Chem., Int. Ed. 60, 26656–26662.
Li, T., Dong, H., Hao, Y., Zhang, Y., Chen, S., Xu, M., Zhou, Y., 2022. Electroanalysis 34, 956–965.
Liu, J., Lu, W., Zhang, L., Yang, J., Yao, Z.-P., He, Y., Li, Y., 2021. Biosens. Bioelectron. 193, 113534.
Liu, X., Meng, J., Ni, K., Guo, R., Xia, F., Xie, J., Li, X., Wen, B., Wu, P., Li, M., Wu, J., Wu, X., Mai, L., Zhao, D., 2020. Cell Rep. Phys. Sci. 1, 100241.
Loget, G., 2019. Curr. Opin. Colloid Interface Sci. 39, 40–50.
Loget, G., Mériadec, C., Dorcet, V., Fabre, B., Vacher, A., Fryars, S., Ababou-Girard, S., 2019. Nat. Commun. 10, 3522.
Medway, S.L., Lucas, C.A., Kowal, A., Nichols, R.J., Johnson, D., 2006. J. Electroanal. Chem. 587, 172–181.
Mu, Y., Jia, D., He, Y., Miao, Y., Wu, H.-L., 2011. Biosens. Bioelectron. 26, 2948–2952.
Nelson, D.L., Cox, M.M., 2021. Lehninger Principles of Biochemistry, eighth ed.
Nguyen, N.S., Das, G., Yoon, H.H., 2016. Biosens. Bioelectron. 77, 372–377.
Pan, T.-M., Lin, J.-C., 2009. Sensor. Actuator. B Chem. 138, 474–479.
Pundir, C.S., Jakhar, S., Narwal, V., 2019. Biosens. Bioelectron. 123, 36–50.
Saada, H., Abdallah, R., Bergamini, J.-F., Fryars, S., Dorcet, V., Joanny, L., Gouttefangeas, F., Ollivier, S., Loget, G., 2020. Chemelectrochem 7, 1155–1159.
Sha, L., Liu, T., Ye, K., Zhu, K., Yan, J., Yin, J., Wang, G., Cao, D., 2020. J. Mater. Chem. 8, 18055–18063.
Shao, G., Zang, Y., Hinds, B.J., 2019. ACS Appl. Nano Mater. 2, 6116–6123.
Shu, J., Qiu, Z., Lv, S., Zhang, K., Tang, D., 2018. Anal. Chem. 90, 2425–2429.
Shu, J., Tang, D., 2020. Anal. Chem. 92, 363–377.
Sun, K., Shen, S., Liang, Y., Burrows, P.E., Mao, S.S., Wang, D., 2014. Chem. Rev. 114, 8662–8719.
Tyagi, M., Tomar, M., Gupta, V., 2013. Biosens. Bioelectron. 41, 110–115.
Urbańczyk, E., Sowa, M., Simka, W., 2016. J. Appl. Electrochem. 46, 1011–1029.
Vedharathinam, V., Botte, G.G., 2013. Electrochim. Acta 108, 660–665.
Wang, B., Cao, J.-T., Liu, Y.-M., 2020. Analyst 145, 1121–1128.
Wang, G., Ling, Y., Lu, X., Wang, H., Qian, F., Tong, Y., Li, Y., 2012. Energy Environ. Sci. 5, 8215–8219.
Yang, Y., Yan, K., Zhang, J., 2017. Electrochim. Acta 228, 28–35.
Yang, Z., Qin, T., Niu, Y., Zhang, Y., Zhang, C., Li, P., Zhu, M., Jia, Y., Li, Q., 2020. Carbon 157, 457–465.
Yoon, J., Lee, E., Lee, D., Oh, T.-S., Yoon, Y.S., Kim, D.-J., 2017. J. Electrochem. Soc. 164, B558–B560.
Yu, Z.-Y., Lang, C.-C., Gao, M.-R., Chen, Y., Fu, Q.-Q., Duan, Y., Yu, S.-H., 2018. Energy Environ. Sci. 11, 1890–1897.
Zhang, J.-Y., He, T., Wang, M., Qi, R., Yan, Y., Dong, Z., Liu, H., Wang, H., Xia, B.Y., 2019. Nano Energy 60, 894–902.
Zhao, W.-W., Xu, J.-J., Chen, H.-Y., 2018. Anal. Chem. 90, 615–627.
Zhao, Y., Yu, J., Xu, G., Sojic, N., Loget, G., 2019. J. Am. Chem. Soc. 141, 13013–13016.
Zhou, Y., Yin, H., Ai, S., 2021. Coord. Chem. Rev. 447, 214156.